A LASER PLATEAU SIZE OPTIMIZATION STRATEGY FOR TMF TESTS

J. R. Riccius, E. B. Zametaev and A. Gernoth - DLR Lampoldshausen, Hardthausen, Germany, 74239

and

W. Schwarz and J. Keppeler - EADS Astrium Space Transportation, Munich, Germany, 81663

1 ABSTRACT

The key component of the Thermo-Mechanical Fatigue (TMF) - test bench at DLR Lampoldshausen is a diode LASER with an optical output power of 11 kW. With the currently built-in LASER optics, heat flux values up to 8 MW/m^2 can be obtained on a LASER beam plateau area of 51 mm x 19 mm. This LASER power density is sufficient to assess the life expectation of nozzle structures and to serve as a validation experiment for nozzle life prediction models. However, for the thermo-mechanical fatigue testing and validation of chamber wall structures, higher LASER power densities are needed. The cost-saving alternative to an increase of the LASER power is to replace the currently available LASER optics by a new LASER optics, leading to a smaller LASER beam plateau size and therefore, resulting in a larger LASER power density. In the current publication, an optimization strategy for the size of the LASER beam plateau area of the new optics module is shown.

2 INTRODUCTION

The strong demand for light-weight structures, which is typical for space transportation systems, leads to a close-to-the-limit design of all involved components – including the rocket engines. The combined thermally and mechanically induced Low Cycle Fatigue of hot gas walls is one of the strongest limiting factors of the life time of key rocket engine components like combustion chambers and expansion nozzles. The development and flight qualification of such components include in line with many other actions CFD and Finite Element analyses of the key components and full scale tests of the whole rocket engine. Thermo-Mechanical Fatigue (TMF) tests can provide essential validation data for these numerical analyses and may even help to reduce the need for full scale tests considerably. Therefore, TMF tests have the potential of both, avoiding failure due to non-validated design analyses as well as saving full scale testing cost.

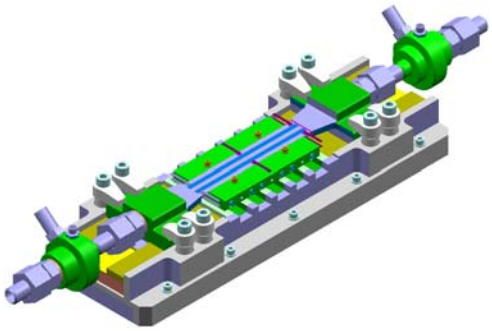

Figure 1: Drawing of the TMF panel structure as tested in the ARIANE 5 FRP programme.

During a TMF test, only a small section of the hot gas wall of the real engine (the so called TMF panel) is tested. The key component of a TMF test bench is a heating device for the hot side of the tested wall component. For medium heat flux applications and a rotatory symmetric test specimen design, a combination of quartz tube radiant heaters and parabolic mirrors can and have been used for jet engine Thermal Barrier Coating (TBC) tests [1], [2].

However, liquid propellant rocket engines are exposed to much higher heat flux densities compared to jet engines. Consequently, realizing relevant environmental conditions inside a TMF bench requires much higher power densities compared to jet engine application. For example, even a local combustion process under ambient pressure does not necessarily provide the high energy density which is necessary for this purpose. Therefore, an optical heating device with a high energy density is required. The remaining options are high power lamps (available as metal halide arc lamps* up to 18 kW, as tungsten wire lamps† up to 24 kW, and as xenon arc lamps‡ up to 30 kW) and high power Laser systems, available on a variety of wave lengths.

Within the frame of the ARIANE 5 Flight Recovery Programme (FRP) – that followed the failure of the maiden flight of the ARIANE 5 ECA launcher in December 2002 – TMF tests were performed by EADS Astrium Space Transportation in cooperation with Volvo Aero Corporation, Snecma Safran and Fraunhofer Institute Dresden to demonstrate the life margin of dump-cooled nozzle structures under relevant thermo-mechanical load conditions [3]. For this purpose, a high power Laser system was used to simulate the heat flux densities observed in full-scale. A combined 10 kW Laser beam was focused by optical lenses on a panel consisting of several metallic tubes as used within the full-scale design. Cold Nitrogen was applied as stipulate coolant fluid, compared to Hydrogen used in the full-scale design. The Laser power was sufficient to expose the required heat load density onto a surface of approximately 70 mm x 30 mm on the tubular panel structure.

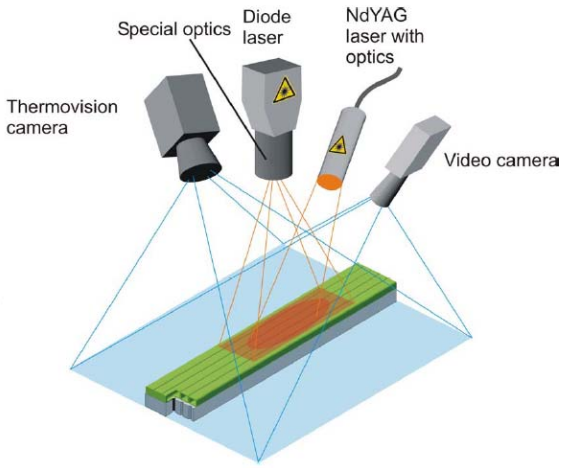

Figure 2: Drawing of the TMF test section as applied in the ARIANE 5 FRP programme.

Figure 1 illustrates the nozzle type TMF panel; Figure 2 shows the test set-up.

The hot wall temperature level and the thermal gradients inside the hot gas wall were adjusted by the coolant mass flow rate, thereby enabling also to exceed the full-scale relevant hot wall temperature level for margin demonstration. Wall temperatures were recorded by means of thermocouples and infrared thermography.

Figure 3 and Figure 4 show snap-shots taken during cyclic testing with cameras, sensitive to the visible and infra red light range, respectively.

Two principle load points were investigated, being characterized by the heat exposure time onto the panel structure:

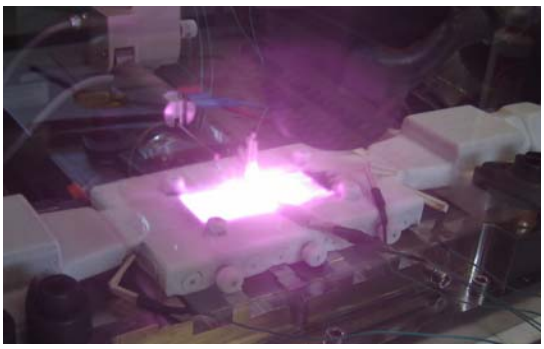

Figure 3: View of a TMF test run during the ARIANE 5 FRP programme.

* URL: http://www.osram.com/_global/pdf/Professional/Display_Optic/Modern_technologies_for_professional_light.pdf; [cited 18 June 2009]

† URL: http://www.arri.de/lighting/europe_asia_australia_africa/tungsten_lampheads/arri_studio_fresnel/arri_studio_t24.html; [cited 18 June 2009]

‡ URL: http://www.ushio.nl/watercooled.html, [cited 19 June 2009]

- Short laser pulses of several seconds to stimulate the low cycle fatigue behavior;
- Long laser pulses to stimulate also creep damage.

The panel structures were exposed to cyclic loadings and tested to failure, being characterized by the first crack appearance observed. These panel test results were used to experimentally demonstrate the margin of the dump-cooling system, as this cannot be achieved at reasonable cost at full-scale engine level. Furthermore, the Finite Element predictions used for the life justification of the full-scale design were compared and validated with the TMF test results.

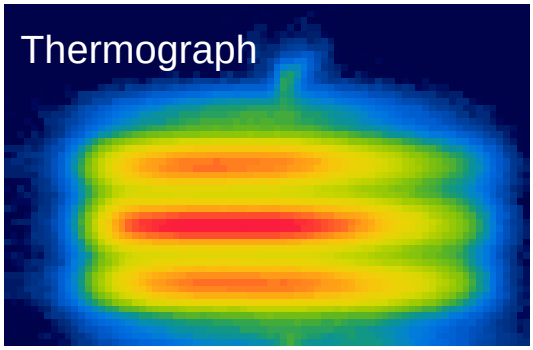

Figure 4: Infrared thermography, obtained at a TMF test run during the ARIANE 5 FRP programme.

3 THE TMF PANEL

In Figure 1, the drawing of a TMF panel designed by ASTRIUM is shown. This panel was used to test a nozzle extension structure. A combustion chamber type TMF panel designed by DLR is shown in the following section.

3.1 TMF panel design

A TMF Panel as shown in Figure 5 was designed by DLR. The dimensions of the thermally loaded wall and the cooling channels (like wall thickness, cooling channel width and height as well as the fin width) were chosen identically to the dimensions in the cylindrical part of a model combustor, tested at DLR Lampoldshausen [4], [5]. Together with the electrically heated cooling channel experiment at DLR Lampoldshausen [6], finally three different experiments with identical cooling channel cross sections and wall dimensions will be available. A possible production technique for this TMF panel is suggested in [7].

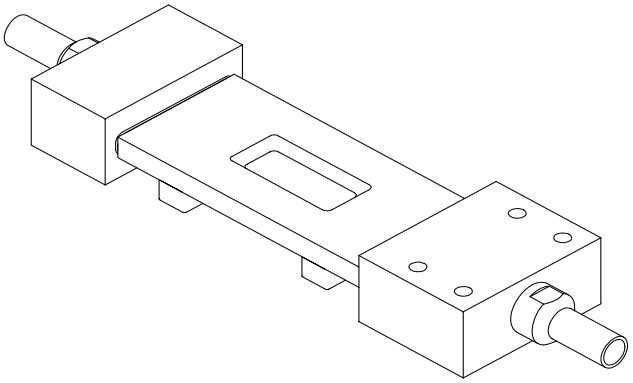

Figure 5: Isometric view of the preliminary combustion chamber type TMF Panel.

4 THE TMF LASER AT DLR LAMPODSHAUSEN WITH CURRENTLY AVAILABLE OPTICS

In this section, the heating device of the TMF test bench at DLR Lampoldshausen – a diode LASER - is discussed. Further subsystems of the TMF test bench at DLR Lampoldshausen like the TMF panel housing as well as the fluid, measurement

Table 1: Key technical parameters of the Laser.

Parameter	value
wavelength	940 nm
optical output power	11 kW
distance from the optics module to the focal plane	415 mm
plateau cross section of the beam at the focal plane	51 mm x 19 mm
homogeneity	better than ± 5%
operational mode	cw

and control systems are discussed in detail in [8]. The key technical parameters of the TMF-LASER as designed and built by DILAS Diodenlaser GmbH [9], [10] are given in Table 1.

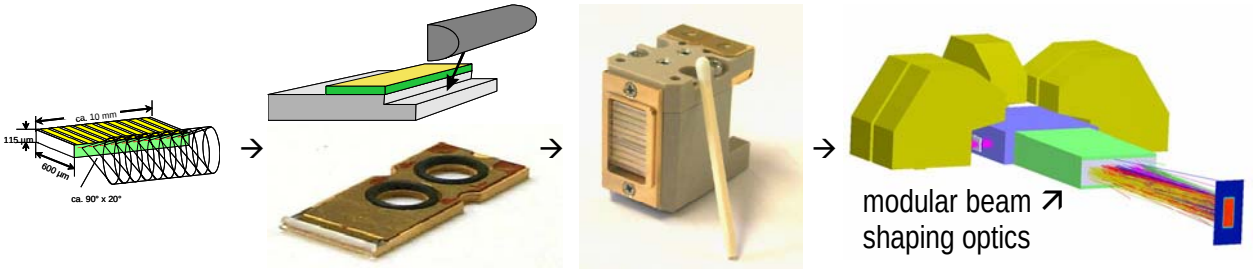

10 Laser diodes	combined with a cylindrical lens & soldered to a cooled copper bar = 1 Laser bar	1 Laser stack module = 10 stacked Laser bars = 100 Laser diodes	Laser head = 20 Laser stack modules = 200 Laser bars = 2000 Laser diodes

Figure 6: Modular structure of the Laser head: Laser diodes (left), Laser bar (middle left), Laser stack module (middle right) and complete Laser head including modular beam shaping optics (right).

The Laser source consists of 20 Laser stack modules as shown in Figure 6 middle right. Grouping four of these stacks together yields to a standard industrial module used e.g. for Laser welding. A combination of five of such standard modules with a beam shaping optics module finally results in the Laser head.

The intensity distribution of the Laser beam at the focal plane with the currently available beam shaping optics, as measured by a transformation of the infrared LASER light into visible light by a fluorescent sheet, is shown in Figure 7. The LASER beam plateau size of 51 mm x 19 mm results in a maximum LASER power density of 8 MW/m^2. As mentioned in section 1 already, the LASER power density has to be increased well above this value by a decrease of the size of the LASER beam plateau size in order to allow tests of chamber wall structures. A strategy for the determination of an optimal plateau size of the LASER beam, shaped by a new optics module is discussed in section 5.

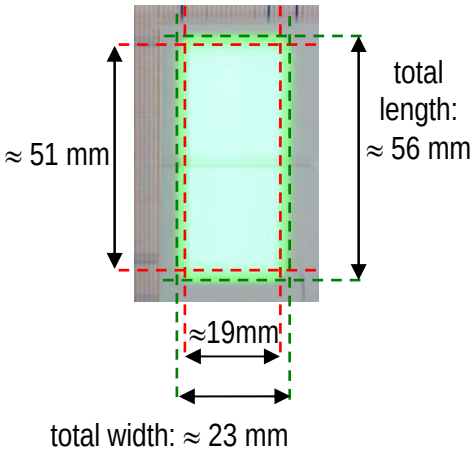

Figure 7. Visualization of the intensity distribution of the Laser beam at the focal plane with an infrared conversion screen.

5 OPTIMIZATION OF THE PLATEAU SIZE OF THE NEW OPTICS MODULE OF THE TMF LASER

5.1 Motivation

The key question for the design of a new modular beam shaping optics module is the determination of the width of the plateau size in the focal plane of the LASER beam:

- Choosing the width of the plateau size too small will result in a strong thermal gradient in tangential direction of the TMF panel. As this direction corresponds to the circumferential direction of the chamber structure, where the thermal gradient is negligible due to symmetry conditions, this results

in an undesirable large difference between the TMF panel and the corresponding combustion chamber structure.

- Choosing the width of the plateau size too large will (due to the limited LASER power) result in a comparatively small thermal gradient in thickness direction of the TMF panel. As this direction corresponds to the radial direction of the chamber structure, where very high thermal gradients occur, this as well results in an undesirable large difference between the TMF panel and the corresponding combustion chamber structure.

Therefore, an optimal size of the plateau cross section of the LASER beam in the focal plane has to be found. For this purpose, an optimization algorithm is used. As the main motivations for the optimization of the Laser beam width are thermal gradients in the TMF panel, such an optimization has to include a numerical model of the TMF panel. In section 5.2, the selection of such a model is discussed.

5.2 CFD versus Finite Element coupled optimization algorithm

In order to keep the thermal gradient in tangential direction of the TMF Panel as low as possible (because this direction is corresponding to the circumferential direction of the combustion chamber, where the thermal gradient is vanishing for symmetry reasons), different coolant mass flow rates in the different cooling channels of the TMF panel are accepted. However, modeling the mass flow through the cooling channels of the TMF panel would require integrating a CFD analysis method into the optimization process. As this would be too time demanding, coolant side film coefficients inside the cooling channels are used instead of mass flow rates. This allows for the optimization to be performed with a (much faster) thermal Finite Element analysis model as described in section 5.3.

5.3 3D Thermal Finite Element model of the TMF panel

Assuming a symmetric design of the TMF panel as well as a symmetric mass flow distribution into the cooling channels, only half of the TMF panel has to be modeled while applying symmetry conditions at the center plane. Therefore, all the meshes in this section show only half of the TMF panel.

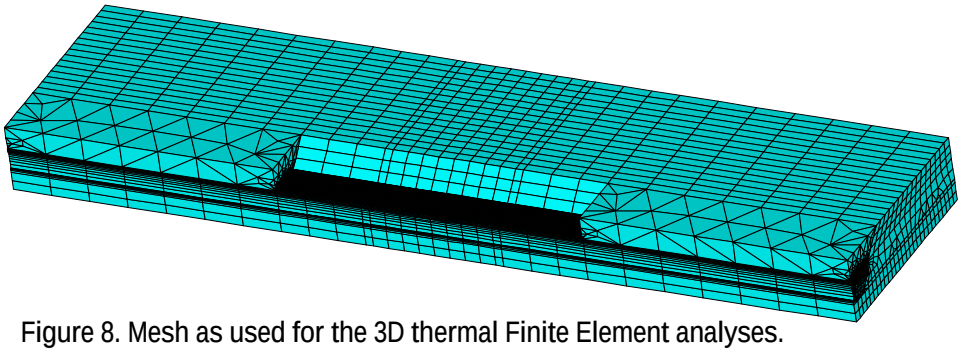

Figure 8. Mesh as used for the 3D thermal Finite Element analyses.

In order to take into account heat conduction in thickness, tangential and axial direction of the TMF panel, a 3D thermal Finite Element model as shown in Figure 8 is used for the optimization analyses.

A TMF panel with 7 cooling channels is considered. Taking into account the above mentioned symmetry of the

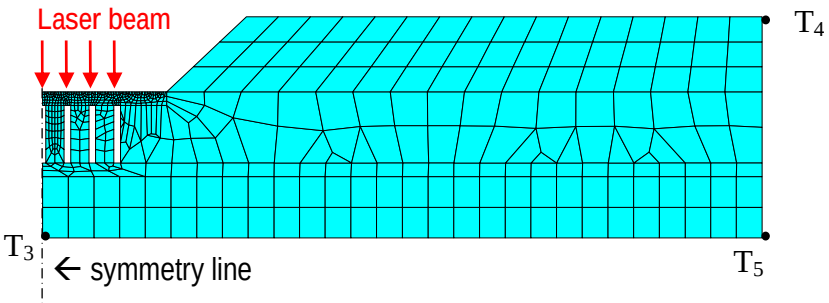

Figure 9. Complete 2D cross section of the 3D Finite Element mesh in the middle of the TMF panel.

TMF-panel, the numerical model contains 3 and a half cooling channels. These cooling channels are visible on the left hand side of the 2D cross section of the Finite Element mesh as shown in Figure 9.

5.4 Optimization Problem Setting

5.4.1 Design variables

The film coefficients are assumed to be constant inside each of the single cooling channels of the model.
Therefore, only four different scalar film coefficient parameters $x_1 = h_{f,1}$, ..., $x_4 = h_{f,4}$ have to be considered as design variables.
Due to LASER optics restrictions, the length of the plateau area of the LASER beam at DLR Lampoldshausen can not be smaller than 32 mm. Therefore, the half width of the plateau area of the LASER beam $x_5 = w_{LASER}/2$ is chosen as the fifth design variable.

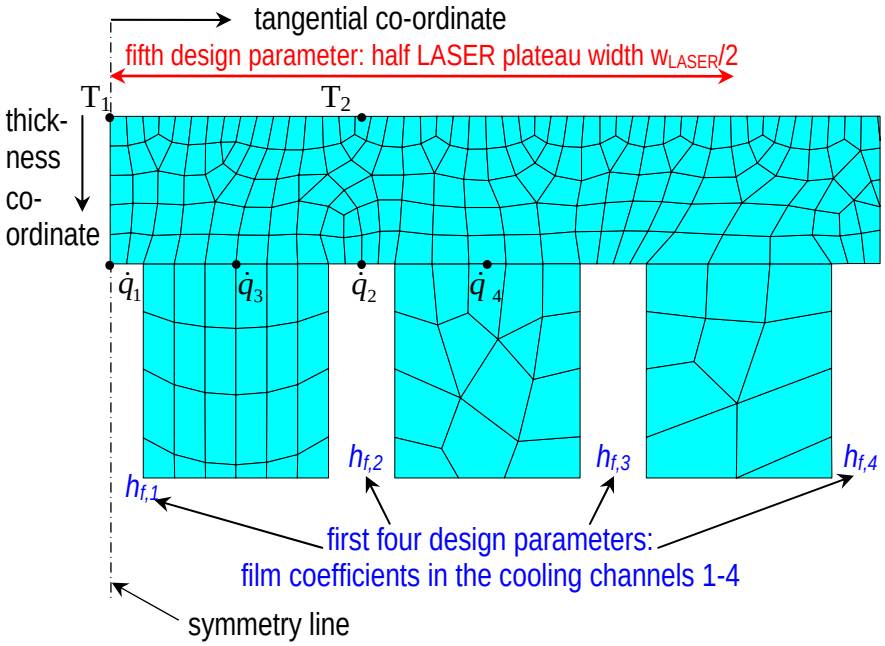

Figure 10. Zoom of the center area of the TMF panel including the Finite Element mesh and the assignments of the film coefficient design parameters $x_1 = h_{f,1}$, ..., $x_4 = h_{f,4}$ as well as the half LASER plateau width design parameter $x_5 = w_{LASER}/2$.

5.4.2 Constraints

Film coefficient constraints: Theoretically, the coolant mass flow could be reduced to zero in case a vanishing film coefficient in this cooling channel would be indicated by the optimization algorithm. However - maintaining a prescribed pressure in this cooling channel would require some coolant to be enclosed inside this blocked cooling channel of the TMF panel as well as in some tubing up to the pressure control valve. As the fluid enclosed in such blocked cooling channels would heat up during the LASER loading, a certain heat flux would occur during the transient phase of the thermal loading of the TMF panel. In case this transient phase lasts longer than the thermal cycle, a zero heat flux condition could not be obtained. Therefore, minimum constraints are specified for the four film coefficient design variables:

$$5\frac{W}{m^2 K} < x_i \;; \qquad i = 1,...,4 \tag{1}$$

LASER width constraints: No constraint was applied to the half LASER plateau width design variable x_5.

Result constraints: A prescribed temperature T_1 should be obtained with a given accuracy at the LASER loaded side of the centerline of the TMF panel. The location of T_1 is indicated in Figure 10. In the work presented in the current publication, a (full scale core stage relevant) temperature of 900 K and an accuracy of 1 K are chosen for this purpose, leading to the following inequality constraint:

$$g_1(x) = 1K^2 - (T_1 - 900K)^2 > 0 \quad (2)$$

5.4.3 Objective function

The objectives of the optimization are:

a) Uniform thermal conditions for temperatures as well as heat flux values at the center area of the TMF panel. This center area is defined as the area containing the three cooling channels in the center of the TMF panel, coinciding with one and a half cooling channels at the symmetry side of the Finite Element model (left-hand side of Figure 9 and Figure 10)

a1) Temperature uniformity condition: For point 2, a temperature T_2 coinciding with the temperature T_1 of point 1 is required.

a2) Heat flux uniformity condition: Due to the constant plateau area of the LASER beam, the heat flux in thickness direction is constant at the LASER loaded side of the TMF panel anyway. Therefore, the heat flux uniformity condition has to require identical heat flux values in thickness direction of the TMF panel at the heated side of the cooling channels as indicated by $\dot{q}_1$ to $\dot{q}_4$ in Figure 10.

b) The largest possible heat flux in thickness direction of the TMF Panel (corresponding on one hand to the LASER power density with the new LASER optics and on the other hand to the radial direction of the hot gas wall of a real combustion chamber or nozzle). Even in case the optimized LASER power density of the new LASER optics should get larger than the heat flux in radial direction of the hot gas wall of the considered real engine – some reserve would be obtained for future engines that are operated by higher chamber pressures and therefore requiring a larger heat flux to keep the wall temperature at an acceptable level. The LASER power can always be reduced in order to get smaller LASER power density values.

c) A low far field temperature in the TMF panel. Due to temperature dependent material properties (e.g. higher Modulus of Elasticity for lower temperatures), this is expected to ensure a stiffer mechanical constraint in tangential direction of the TMF panel and therefore, a better coincidence with the compressive loading of the hot gas wall due to the hoop stress of the outer layer of the engine.

Objectives a1) and a2) could either be taken into account by constraints or directly in the objective function. In order to avoid that design sets are marked as infeasible by the optimization program in case conditions a1) and a2) can not be fully met, these objectives are included in the objective function. Weighting factors w_i for these terms had to be adjusted manually. Following this approach, the objectives a), b) and c) can e.g. be obtained by a minimization of one of the following objective functions:

i) Narrow uniformity condition objective function:

$$f_1(x) = w_1(T_2 - 900K)^2 + w_2(\dot{q}_{1,thicknessdirection} - \dot{q}_{2,thickessdirection})^2 + w_3 T_3^{\,2} + w_4 T_4^{\,2} + w_5 T_5^{\,2} \xrightarrow[x]{} \min \quad (3)$$

ii) Wide uniformity condition objective function:

$$f_2(x) = w_1(T_2 - 900K)^2 + w_2(\dot{q}_{3,thicknessdirection} - \dot{q}_{4,thickessdirection})^2 + w_3 T_3^{\,2} + w_4 T_4^{\,2} + w_5 T_5^{\,2} \xrightarrow[x]{} \min \quad (4)$$

Together with the constraint as given by equation (2), the first term of these objective functions "pushes" the design into similar temperatures T_1 and T_2, leading to a temperature uniformity region between points 1 and 2 of the TMF panel (objective a1).
The second term of these objective functions leads to a design with similar heat flux values $\dot{q}_{1,thicknessdirection}$ and $\dot{q}_{2,thicknessdirection}$ for equation (3) or $\dot{q}_{3,thicknessdirection}$ and $\dot{q}_{4,thicknessdirection}$ for equation (4) (objective a2).
The third term of these objective functions leads to a strong gradient in thickness direction of the TMF panel (objective b).
The fourth and fifth term of these objective functions lead to low far field temperatures T_4 and T_5 (objective c)

5.5 Applied optimization method

The applied optimization procedure consists of two steps: Transformation of the constrained minimisation problem into an unconstrained minimisation problem by means of penalty terms and solution of the unconstrained minimisation problem by a standard Conjugate Gradient method.

5.5.1 Transformation of the constrained minimisation problem into an unconstrained minimisation problem

Penalty functions X and G are used in order to transform the constrained minimisation problem (1), (2), (3) or alternatively (1), (2), (4), into an unconstrained minimisation problem with the dimensionless objective function $F(x, p)$:

$$F(x,p) = \frac{f(x)}{f_0} + \sum_{i=1}^{4} X(x_i) + pG(g_1(x)) \tag{5}$$

with:

f_0	reference objective function value
p	adaptively chosen penalty parameter
$X(x_i)$	exterior penalty functions for design variables
$G(g_1(x))$	extended interior penalty function for state variable function g_1

5.5.2 Solution of the unconstrained minimisation problem

Each iteration step of a gradient based optimization procedure can be split into 3 parts: Approximation of the gradient; choice of a gradient based search direction and update of the design variables. For the optimization of the model combustion chamber, the Conjugate Gradient method according to Polak and Ribiére [11] was used.

Approximation of the gradient of the objective function F:
As the gradient can not be determined analytically, a forward difference quotient is used to approximate the gradient of the dimensionless objective function F of the unconstrained minimisation problem:

$$\nabla F = \left(\frac{\partial F(x)}{\partial x_1}, ..., \frac{\partial F(x)}{\partial x_5} \right)^T \tag{6}$$

$$\frac{\partial F(x)}{\partial x_i} \approx \frac{F(x + \Delta x_i e_i) - F(x)}{\Delta x_i} \tag{7}$$

with:

e_i vector with 1 in its i-th component and 0 for all other components

Δx_i small increment for i-th design variable

- Determination of a search direction

At the first iteration step, the negative gradient is used as a search direction d_0:

$$d^0 = -\nabla F(x^0) \tag{8}$$

with: $x^0 = (x_1{}^0, x_2{}^0, x_3{}^0, x_4{}^0, x_5{}^0)^T$: initial design variable vector.

At subsequent iterations, the negative gradient is modified by adding the previous search direction d_{j-1}, scaled by a factor r_j :

$$d^j = -\nabla F(x^j) + r^j d^{j-1} \tag{9}$$

$$r^j = \frac{(\nabla F(x^j) - \nabla (F(x^{j-1})) \cdot \nabla F(x^j)}{\nabla F(x^{j-1}) \cdot \nabla F(x^{j-1})} \tag{10}$$

Occasionally, the Conjugate Gradient algorithm is restarted by choosing the steepest descent search direction according to equation (8) instead of the conjugated direction.

- Update of the design variable vector

Finally, the new design variable vector x^{j+1} is obtained by the following equation:

$$x^{j+1} = x^j + s^j d^j, \qquad j = 0,1,2,... \tag{11}$$

The line search parameter s^j corresponds to the minimum value of F in the search direction d^j.

5.6 Chosen parameter values

The key geometrical dimensions of the TMF panel such as the width w_c of the cooling channels; the height h_c of the cooling channels and the thickness t_w of the LASER heated wall are chosen identical to the HARCC geometry as used for other experiments at DLR Lampoldshausen [4], [5], [6].

Values as given in Table 2 are used as initial values of the design parameters and the weighting factors in the objective function.

Table 2: Initial design parameter values and weighting factors as used for the optimization.

parameter group	parameter	unit	value (narrow)	value (wide)
initial film coefficients	$x_1^{\,0} = h_{f,1}^{\,0}$ (in the centerline cooling channel)	$\frac{W}{m^2 K}$	15500	5500
	$x_2^{\,0} = h_{f,2}^{\,0}$		600	600
	$x_3^{\,0} = h_{f,3}^{\,0}$		840	840
	$x_4^{\,0} = h_{f,4}^{\,0}$ (in the outer cooling channel)		14100	4100
	initial half width of the LASER beam in the focal plane	mm	6.7	6.7
weighting factors of the different terms of the objective function	w_1		1000	1000
	w_2		1	1
	w_3		1	1
	w_4		1	1
	w_5		1	1

5.7 Optimization results

5.7.1 Evolution of the objective function and the design parameters

The diagram on the left-hand side of Figure 11 shows the strong reduction of the objective function during the optimization process – indicating a correct function of the optimization algorithm, whereas the diagram on the right-hand side of Figure 11 contains the main result of the optimization, indicating an optimal LASER beam plateau width of 9.7 mm for the narrow uniformity design and 13.6 mm for the wide uniformity design.

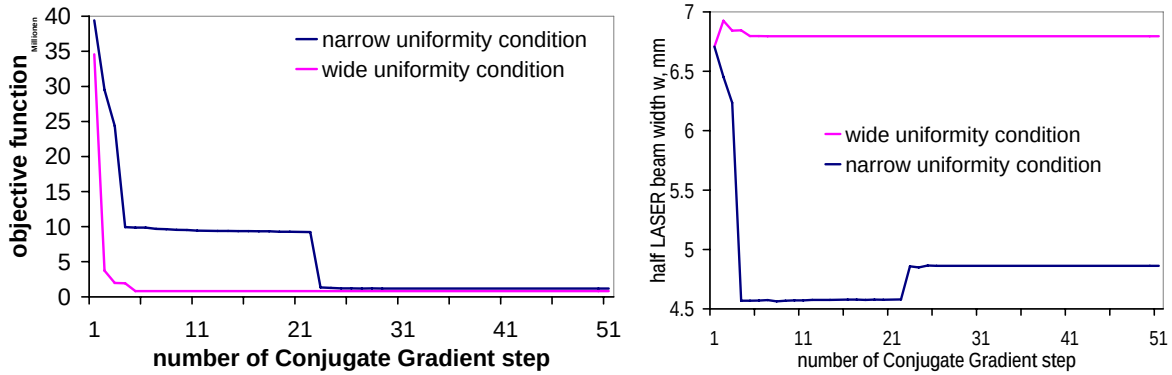

Figure 11. Left: Evolution of the objective function; Right: evolution of the half LASER plateau width design parameter in dependency on the number of Conjugate Gradient steps.

The evolution of the four film coefficient design parameters during the optimization process is shown in Figure 12. For both, the narrow as well as the wide uniformity condition designs, the largest film coefficient is assigned to the outer channel (no. 4).This is obviously caused by terms 4 and 5 of the objective function, corresponding to objective c (low far field temperature of the TMF panel).

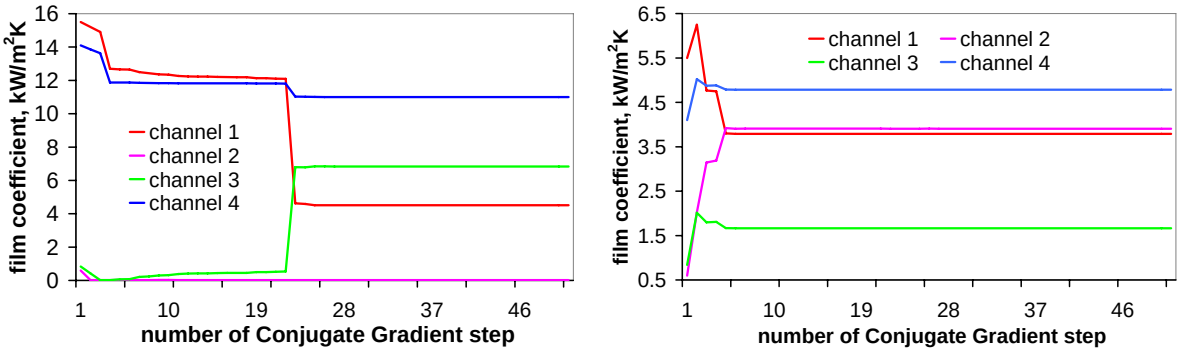

Figure 12: Evolution of the film coefficient design parameters in dependency on the number of Conjugate Gradient steps; Left: for narrow uniformity condition: Right: for the wide uniformity condition.

5.7.2 Temperature and LASER power density line plots of the two optimized designs

In Figure 13, the LASER power density distributions in tangential direction of the middle cross section of the TMF panel and the resulting temperature distributions are shown for both optimized designs. The optimization result by use of the narrow uniformity condition objective function (3) shows a higher LASER power density in the plateau region of more than 20 MW/m², but also a temperature drop in the 2nd cooling channel in comparison to the centerline cooling channel of about 25K. This temperature drop from the centerline to the 2nd cooling channel is with 5K much smaller in case the wide uniformity condition objective function (4) is used for the optimization. However, this results in a lower LASER power density in the plateau region of slightly above 15 MW/m².

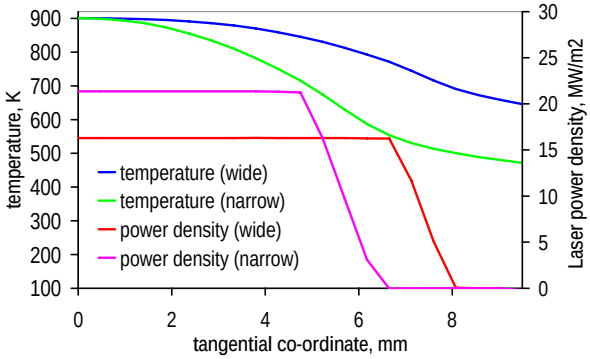

Figure 13. Tangential variation of the temperature on the LASER loaded side of the TMF panel and LASER power density distribution for 2 optimized designs.

5.7.3 3D Thermal field of the TMF panel with optimized design parameters

The 3D plots of the thermal field of the TMF panel in Figure 14 show a globally lower temperature for the narrow uniformity condition optimization.

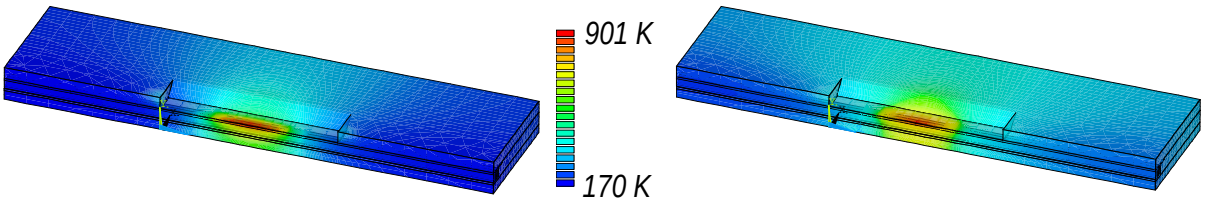

Figure 14. 3D thermal fields in the TMF panel. Left: with narrow uniformity condition optimization; Right: with wide uniformity condition optimization.

5.7.4 2D Thermal field of the TMF panel with optimized design parameters

The thermal field on the right-hand side of Figure 15 (as obtained by the wide uniformity condition optimization) shows in comparison to the thermal field shown on the left-hand side of Figure 15 (as obtained by the narrow uniformity condition optimization) a much smaller variation of the temperature in tangential direction of the TMF panel – increasing the probability that the LASER heated wall in the vicinity of the centerline cooling channel of the TMF panel "gets" symmetry boundary conditions from the bordering cooling channels – such as in a real combustion chamber.

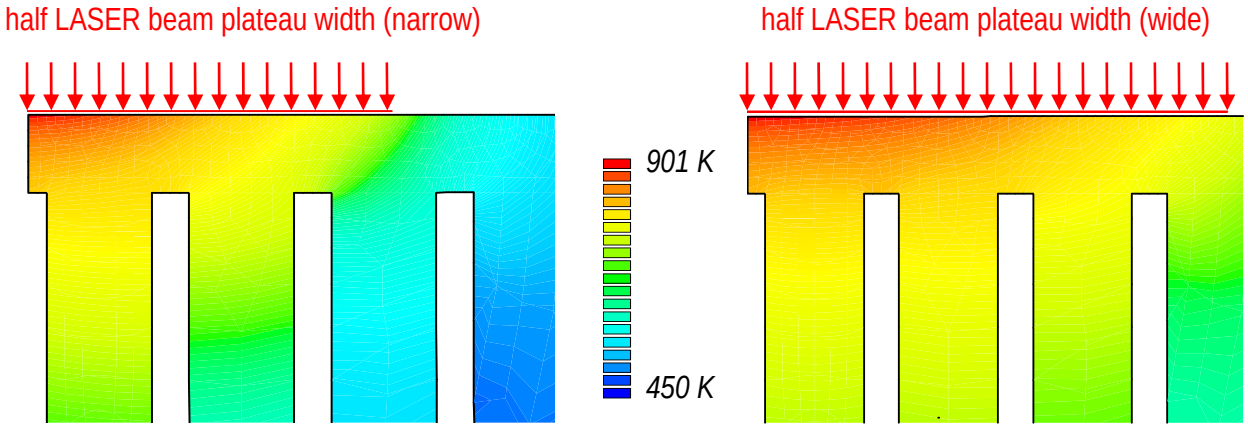

Figure 15. 2D thermal fields in the center cross section of the TMF panel. Left: obtained by the narrow uniformity condition optimization; Right: obtained by the wide uniformity condition optimization.

6 CONCLUSION AND OUTLOOK

6.1 Optimization results

Two different optimized LASER beam plateau widths were obtained by running a Conjugate Gradient optimization algorithm with slightly modified objective functions: The narrow width design leads to (a very desirable) higher heat flux value in thickness direction of the TMF panel. However, this advantage has to be paid for by a stronger temperature variation of the LASER heated surface of the TMF panel in the vicinity of the three inner cooling channels of the TMF panel (corresponding to the two cooling channels in the vicinity of the symmetry side of the TMF panel model).

6.2 Future TMF panel tests

As soon as the TMF test bench at DLR Lampoldshausen is fully operable with the currently available LASER optics, tests with nozzle type TMF panels can be performed. The results of these TMF tests can then be used for the verification of CFD and Finite Element nozzle models as well as for the pre qualification of production technologies recently applied to nozzles (e.g. Laser welding [12] and sandwich technology [13]) and/or recently applied thermal barrier coatings [14] with respect to the cyclic thermo-mechanical fatigue of these nozzle production technologies and/or coatings.

As soon as the higher concentrating LASER optics is available at DLR Lampoldshausen, also combustion chamber wall structures can be tested. The results of these TMF tests can then be used for the verification of CFD and Finite Element combustion chamber wall models as well as for the pre qualification of recently developed combustion chamber wall geometries (e.g. elastic liner [15] and high aspect ratio cooling channels [5]), recently applied combustion chamber wall production technologies (e.g. brazing [16]), new combustion chamber wall materials (e.g. CuCrNb [17]) as well as material production technologies recently

used to manufacture combustion chamber walls (e.g. vacuum plasma spraying [18]) with respect to the cyclic thermo-mechanical fatigue of these combustion chamber wall geometries, materials and/ or production technologies.

7 REFERENCES

[1] Bartsch, M.; Baufeld, B.; and Heinzelmann, M., "CMSX-4 with Thermal Barrier Coating under Thermal Gradient Mechanical Fatigue," 9th International Conference on Fatigue, 2006.

[2] Baufeld, B.; and Bartsch, M., "Temperature Measurement in Thermal Gradient Mechanical Fatigue Testing of Material Systems with Coatings," Proceedings of a Symposium sponsored by Engineering Conferences International, edited by Fuchs, G. E.; James, A. W.; Gabb, T.; McLean, M.; and Harada, H., Advanced Materials and Processes for Gas Turbines, 22 – 26 September 2002, p. 75 – 82.

[3] Ferrandon, O.; James, P.; Girard, P.; Terhardt, M.; Blasi, R.; Johnsson, R.; and Damgaard, T., "VULCAIN 2 Nozzle Extension: Integrated European Team and Advanced Computational Models to the Service of Nozzle Design," 41st AIAA/ASME/SAE/ASEE Joint Propulsion Conference, 2005.

[4] Suslov, D.; Woschnak, A.; Sender, J.; and Oschwald, M., "Test Specimen Design and Measurement Technique for Investigation of Heat Transfer Processes in Cooling Channels of Rocket Engines under Real Thermal Conditions," 39th AIAA/ASME/SAE/ASEE Joint Propulsion Conference, 20 - 23 July 2003.

[5] Woschnak, A.; Suslov, D.; and Oschwald, M., "Experimental and Numerical Investigations of Thermal Stratification Effects," 39th AIAA/ASME/SAE/ASEE Joint Propulsion Conference, 20 - 23 July 2003.

[6] Torres, Y., "Heat and Mass Transfers in Curved Cooling Channels of Rocket Engines," PhD Thesis, L´Université de Valenciennes et du Hainaut Cambrésis, Ecole Doctorale ED72, October 2008.

[7] Riccius, J.; Gernoth, A.; Suslova, E.; Böhm, C.; Zametaev, E.; Haidn, O.; Brummer, L.; Mewes, B.; Knab, O.; Terhardt, M.; and Hagemann, G., "TMF: Laser Application for a Close-to-Reality Simulation of Thermo-Mechanical Fatigue Processes in Rocket Engines," 2nd European Conference for Aerospace Sciences (EUCASS), 1-5 July, 2007.

[8] Gernoth, A.; Riccius, J.R.; Haidn, O.J.; Brummer, L.; Mewes, B.; and Quering, K., "TMF panel tests: close-to-reality simulation of thermo-mechanical fatigue processes in heat-loaded walls," AIAA 2008-5237, 44th AIAA/ASME/SAE/ASEE Joint Propulsion Conference & Exhibit 21 - 23 July 2008, Hartford, CT

[9] Köhler, B.; Noeske, A.; Kindervater, T.; Wessollek, A.; Brand T.; and Biesenbach, J., "11 kW direct diode laser system with homogenized 55 x 20 mm² Top-Hat intensity distribution," Photonics West; 2007.

[10] Overton, G., "LASER-BEAM SHAPING: Diode-laser system yields 11 kW homogenized output," Laser Focus World, Volume 43, Issue 5, May 2005, URL: http://www.laserfocusworld.com/display_article/292380/12/ARTCL/none/News/LASER-BEAM-SHAPING:-Diode-laser-system-yields-11-kW-homogenized-outpue; [cited 30 June 2009].

[11] Polak, E.; and Ribiére, G., "Note sur la convergence de méthodes de directions conjuguées," Revue Française d´Informatique et de Recherche Opérationnelle 16, 35-43, 1969

[12] Damgaard, T.; Brox, L.; and Hallberg, M., "Demonstration of a Laser Welded Channel Wall Nozzle - Vulcain 2 Scale," 42nd AIAA/ASME/SAE/ASEE Joint Propulsion Conference & Exhibit, 2006.

[13] Emvin, P., "The V2+ Nozzle Extension Demo: A milestone on the route to sandwich nozzle production," 57th International Astronautical Congress, 2-6 October, 2006.

[14] Winterfeldt, L.; Laumert, B.; Tano, R.; Blasi, R.; and Hagemann, G., "Redesign of the Vulcain 2 Nozzle

Extension," 41st AIAA/ASME/SAE/ASEE Joint Propulsion Conference & Exhibit, 10 – 13 July 2005.

[15] Immich, H.; Kretschmer, J.; and Preclik, D., "Thrust Chamber Technology Developments for Future Launch Vehicle Liquid Rocket Engines," 37th AIAA/ASME/SAE/ASEE Joint Propulsion Conference & Exhibit, 2001.

[16] Preclik, D.; Hagemann, G.; and Kretschmer, J., "Technology Efforts towards Low-Cost Thrust Chambers," 37th AIAA/ASME/SAE/ASEE Joint Propulsion Conference & Exhibit, 20-23 July 2003.

[17] Ellis, D. L., "GRCop-84: A High-Temperature Copper Alloy for High-Heat-Flux Applications," NASA/TM—2005-213566, Glenn Research Center, Cleveland, Ohio, 2005.

[18] Thomas, J. L.; Cornu, D.; Choulant, M.; Verdy, C.; and Coddet, C., "Vacuum Plasma Spray Process applied to high thickness components for Liquid Rocket Engine," 41st AIAA/ASME/SAE/ASEE Joint Propulsion Conference & Exhibit, 10 - 13 July 2005.